Research Square

Preprints are preliminary reports that have not undergone peer review.
They should not be considered conclusive, used to inform clinical practice,
or referenced by the media as validated information.

Synergistic Enhancement of Thermal Stability in Epoxy Nanocomposites via IPN Formation and GnPs/MWCNTs Hybrids

Afrooz Molaei
Institute for Color Science and Technology
Ali Jannesari
Jannesari-a@icrc.ac.ir

Institute for Color Science and Technology

Research Article

Keywords: Interpenetrating Polymer Network (IPN), Thermal Properties, Nanocomposites, Degradation, Thermal Gravity Analysis (TGA)

Posted Date: June 12th, 2026

DOI: https://doi.org/10.21203/rs.3.rs-9667996/v1

License: This work is licensed under a Creative Commons Attribution 4.0 International License.
Read Full License

Additional Declarations: No competing interests reported.

Version of Record: A version of this preprint was published at Polymer Bulletin on August 12th, 2026.
See the published version at https://doi.org/10.1007/s00289-026-06635-8.

Synergistic Enhancement of Thermal Stability in Epoxy Nanocomposites via IPN Formation and GnPs/MWCNTs Hybrids

Afrooz Molaei [a], Ali Jannesari [a]*

[a] Department of Resins and Additives, Institute for Color Science and Technology, Tehran, Iran.

*Corresponding Author. Tel: +989123548097

Email: Jannesari-a@icrc.ac.ir (Ali Jannesari)

Abstract

This study investigates the thermal properties and microhardness of epoxy/vinyl ester (EP/VE) interpenetrating polymer networks (IPNs) containing hybrid nanofillers comprising graphene nanosheets (GnPs) and multi-walled carbon nanotubes (MWCNTs). An equal weight ratio mixture of two compatible resins with similar chemical structures but different curing mechanisms, namely epoxy and vinyl ester resins, both based on bisphenol-A, was used to fabricate the IPN matrix. Thermogravimetric analysis (TGA) and differential thermal analysis (DTA) were used to evaluate the effects of the type and amount of nanofillers based on carbon allotropes on the thermal degradation behavior of the resulting nanocomposites. The DTG thermogram of the IPN sample showed a single degradation peak, indicating the formation of a full interpenetrating polymer network and high compatibility between its constituent resin components, and the absence of detectable phase separation. Changes in TGA and DTG parameters of IPN samples containing hybrid nanofillers, compared to those without them, indicate that these nanofillers have improved the IPN's thermal stability. The nanocomposite containing 0.1 wt% GnPs/MWCNTs hybrid exhibits optimal performance and the highest fire retardancy, with a limiting oxygen index (LOI) of 20.17%. Microhardness measurements revealed that the IPN system exhibited hardness values comparable to those of the pure epoxy resin, indicating that mechanical integrity was maintained while also improving thermal properties.

Highlights

- Interpenetrating polymer networks combine crosslinked polymers to tailor material characteristics.
- A hybrid of Graphene nanoplatelets (GnPs)/multi-walled carbon nanotubes (MWCNTs) improves the thermal stability of IPNs.
- Thermal gravimetric analysis assesses the stability and compatibility of IPNs and nanocomposites.
- IPNGC1 (0.1 wt% GnP/MWCNT) exhibits high fire retardancy, with a limiting oxygen index (LOI) of 20.17%.
- DTG thermograms indicate homogenous IPN systems with a single peak.

Keywords: Interpenetrating Polymer Network (IPN), Thermal Properties, Nanocomposites, Degradation, Thermal Gravity Analysis (TGA)

1. Introduction

Polymer blends, such as interpenetrating polymer networks (IPNs), which combine two or more crosslinked polymers, offer unique opportunities to customize material properties superior to those of their components and achieve improved performance [1-3]. The Interpenetrating polymer networks form when at least one polymer is polymerized or crosslinked in the presence of another. This process creates an interpenetrated structure, which can improve toughness, impact resistance, and damping properties. As a result, IPNs are suitable as matrices for composite and vibration control applications [4–11]. Sperling defined IPNs as systems where two or more polymers are synthesized in a network form [12], and Utracki noted that the thickness of the network strands can range from 10 to 1000 nm [13].

Two resins, epoxy and vinyl ester based on bisphenol A, have attracted the attention of researchers as one of the best-known IPN systems due to their compatibility, resulting from their similar chemical structures and different curing mechanisms. These resin mixtures have led to the creation of materials with remarkable mechanical, thermal, and rheological behaviors [14-18]. The

properties of these resin blends are significantly affected by their morphology, whether in continuous or dispersed form. Despite the improvements offered by epoxy and vinyl ester IPNs, specific properties often require further enhancements, motivating the use of micro- and nanoscale fillers to tune IPN characteristics [19–29].

Some papers have systematically investigated how filler type, dispersion, and concentration affect the thermal stability, glass transition temperature, and conductivity of epoxy-based IPNs. Hiremath et al. studied glass fiber reinforced epoxy-vinyl ester IPN (GEVIPN) composites [30]. With increasing post-curing temperature, DMTA analysis results showed that the glass transition temperature (Tg) of these GEVIPN composites increased, indicating higher crosslink density and improved bonding between the IPN matrix and glass fibers. Optimal post-curing at 200 °C resulted in lower loss modulus and tanδ peak heights, further confirming strong interfacial bonding that affects the composite's thermal behavior and energy dissipation. Molaei et al. investigated the structure and viscoelastic behavior of epoxy/vinyl ester IPN nanocomposites containing graphene nanoplatelets (GnPs) and multi-walled carbon nanotubes (MWCNTs) [31]. Their dynamic mechanical thermal analysis (DMTA) revealed that 0.5 wt% MWCNTs yielded the highest glass transition temperature (Tg) of 124.81°C. This result indicated enhanced thermal stiffness. Yang et al. constructed in situ IPN structures from epoxy and vinyl ester resins and examined the effect of octavinyl polyhedral oligomeric silsesquioxane (EPOSS) as a nanoscale dispersion on thermal and mechanical performance [32]. They found that well-dispersed nanofiller networks can simultaneously improve toughness and thermal properties, especially when phase separation is avoided. Their findings stressed the importance of controlling the filler–polymer interface. Dean et al. provided foundational insights into the cure kinetics and morphology of epoxy–vinyl ester IPNs [33]. Through near-infrared and rheological studies, they demonstrated how fillers and the

interplay between polymer networks affect network formation and vitrification. These factors ultimately affect the thermal and mechanical properties of IPNs. These studies demonstrate that the type, content, and dispersion state of these nanofillers are crucial for optimizing the thermal properties of epoxy-vinyl ester IPNs. The use of hybrid nanofillers, particularly a combination of GnPs and MWCNTs, results in the development of multifunctional IPNs with superior thermal properties. Combining nanofillers with different geometries can yield enhanced properties compared to single nanofillers. For instance, Afolabi et al. and Wang et al. demonstrated that combining carbon nanotubes with graphene nanoplatelets creates a co-supporting network in which nanotubes bridge the gaps between graphene sheets [34–35]. Jen et al. and Yang et al. further explored the synergistic effects of hybrid nanofillers on the electrical and thermomechanical properties of epoxy composites [36–37].

In this paper, we examine the incorporation of multi-walled carbon nanotubes and graphene nanoplatelets and their effects on the thermal properties of vinyl ester/epoxy IPN thermosets. These nanofillers are examined both individually and as hybrid systems. This study aims to compare their effects on the thermal degradation behavior of IPN-based nanocomposites. The aim is to identify optimal content and combinations for enhanced thermal properties. The IPN system considered in this study consists of a mixture of epoxy resin with bisphenol-A structure cured with methyl tetrahydrophthalic anhydride (MTHPA) and vinyl ester resin with bisphenol-A structure initiated with methyl ethyl ketone peroxide (MEKP) in a mass ratio of 1:1. In this study, the effect of the type and content of nanofillers based on carbon allotropes on the results of thermogravimetric analysis (TGA) and microhardness test is investigated. It characterizes the dispersion and arrangement of nanofillers within the matrix using scanning electron microscopy (SEM).

2. Experimental

2.1. Materials

A bisphenol-A diglycidyl type epoxy resin (EP) (Epon 828 with epoxide equivalent weight of 170–210 g/eqv) was obtained from Hexion Specialty Chemicals, Inc. (150 East Board Street, Columbus, Ohio, 43215, USA) and used as received. Methyl tetrahydrophthalic anhydride (MTHPA) and 1-methylimidazole (Mi), used as a curative and an accelerator, respectively, were obtained from Huntsman Advanced Materials GmbH (Klybeckstrasse 2004057, Basel, Switzerland) for curing the EP resin. For EP/MTHPA, the EP/curing agent ratio was set at 1/0.92, and 2 phr of Mi was used. The vinyl ester resin (VE) was bisphenol-A type (Swancor 901; styrene content: 45 wt.%), a product of Swancor Co., Ltd. (no. 9 Industry South 6 Road, Nantou City 54066, Taiwan), and was provided for this study. For the VE (vinyl ester resin) curing reaction, 2 phr Methyl ethyl ketone peroxide (Butanox LPT-IN) (Nouryon HQ, Haaksbergweg 88, De Oliphant Building, Floor 14 and 15, 1101 BZ, Amsterdam, The Netherlands) was consumed. For all samples, the ratio of EP/VE was considered to be constant (1:1). NC7000 MWCNTs was supplied by Belgium Nanocyl SA (Rue de l'Essor, 4 B-5060, Sambreville, Belgium) with an average length of 1.5 μm, an average diameter of 9.5 nm, a Brunauer–Emmett–Teller (BET) surface area of 250–300 m^2/g, and a purity of 90% were used as the nanofiller without further purification. The GnPs used in this study, with the trade name of xGnP® Graphene Nanoplatelets-Grade C, was obtained from XG Sciences Inc. (101 Grand Oak Drive, Lansing, MI 48911, USA). The GnPs diameter is about two μm, and its thickness is a few nanometers. The purities of GnPs are higher than 99.5%, and their BET surface area is 500 m^2/g. Afcona 4701, as a dispersing agent, was supplied by Afcona Polymers Co., Ltd. (21 Jalan Anggerik Mokara, 31/47 Kota Kemuning 40460 Shah Alam, Selangor, Malaysia). Isopropyl alcohol, used as the solvent, was purchased

from Merck (Frankfurter Str. 250, 64293 Darmstadt, Germany) and was used as received without further purification.

2.2. Sample preparation

2.2.1. IPN and Nanocomposite samples preparation

Firstly, the resin blends were prepared by physically combining epoxy and vinyl ester resins. The ratio of each resin system was maintained at the typical level as in the IPN (50:50). Next, MEKP and MTHPA were added, respectively, and the solution was homogenized using a homogenizer. As a final point, Mi was added as an EP accelerator, and the resin mixture was poured into a beaker, degassed under vacuum, and then poured into open silicone molds. The curing regime for the produced sample (3 mm in length, 3 mm in width, and 1 mm in thickness) was as follows: 80 °C for 4 hours and 120 °C for 2 hours.

To prepare nanocomposite samples, solution method was used [38-39]. The dispersing agent Afcona 4701 was used to improve dispersion and stability. The dispersing agent was added to the isopropyl alcohol during the manufacturing process. The mixture was then stirred for 30 minutes using a mechanical stirrer. The nano-fillers, including GnPs and MWCNTs, were individually added to the prepared solution. The obtained mixture was agitated with a mechanical stirrer for 10 minutes and then subjected to ultrasonication for 30 minutes in an ice/water bath to achieve uniform dispersion and distribution of the nanoparticles in the isopropyl alcohol solution. Afterward, EP resin was added to the mixture and heated to 80°C while agitating until the isopropyl alcohol evaporated. Next, VE resin was added to the mixture and agitated for 30 minutes in an ice/water bath. Finally, curing agents were added to the mixture, and the mixture was agitated for 15 minutes with a mechanical stirrer. Further details on nanofiller concentrations and sample coding are provided in Table 1. The prepared nanocomposite materials were cast into open silicone

molds, degassed under vacuum, and cured. The curing regime for the produced samples (3 mm in length, 3 mm in width, and 1 mm in thickness) was as follows: 80 °C for 4 hours, followed by 120 °C for 2 hours. For DSC scanning, the EP and VE samples, as well as the 50:50 EP: VE mixture (by weight, corresponding to the IPN sample), were prepared by mixing with their respective curatives.

Table 1. The sample compositions are given by weight percentage.

NO.	Sample	Resin systems					Nanofillers		Dispersing agent
		EP	MTHPA	Mi	VE	MEKP	MWCNTs	GnPs	Afcona 4701
1	IPN	25.832	23.845	0.323	49.018	0.982	0	0	0
2	IPNG01	25.827	23.840	0.323	49.008	0.982	0	0.01	0.01
3	IPNG1	25.781	23.797	0.322	48.920	0.980	0	0.1	0.1
4	IPNG5	25.574	23.607	0.319	48.528	0.972	0	0.5	0.5
5	IPNC01	25.827	23.840	0.323	49.008	0.982	0.01	0	0.01
6	IPNC1	25.781	23.797	0.322	48.920	0.980	0.1	0	0.1
7	IPNC5	25.574	23.607	0.319	48.528	0.972	0.5	0	0.5

2.3. Characterization

Thermogravimetric analyses were performed using a differential thermal thermogravimetric apparatus (Diamond TG/DTA SII thermogravimetric analyzer, manufactured by PerkinElmer Inc., USA) over the temperature range of 30–600℃ under a N_2 atmosphere to exclude complexities originating from oxidation reactions. The thermal degradation of the samples after curing was

evaluated using a non-isothermal method at a heating rate of 10 °C/min. Differential scanning calorimetry (DSC) was used to study the curing behavior of the samples. This study was carried out using a NETZSCH DSC 214 instrument operating over the temperature range of -20 °C to 300 °C, with a heating rate of 10 °C/min under a dry nitrogen flow.

Thermoanalytical tests were carried out using approximately 12 ± 1 mg of specimens encapsulated in standard pans. Scanning electron microscopy (SEM, LEO 1455VP instrument, manufactured by LEO Electron Microscopy Ltd., Cambridge, UK; equipped with an Everhart-Thornley secondary electron detector) was utilized to evaluate the morphology of the nanocomposites (15 KV). The specimens were prepared for SEM by coating a layer of gold on their surface fractures. Micro-hardness was measured using a micro-hardness tester (HMV2; Hardness Test Machine; Hardness Ark-600, Mitutoyo Co., Kawasaki, Japan). Vickers hardness measurements HV0.1 were performed using an indentation load of 0.9807 N for 10 seconds. For micro-hardness testing, ten observations were taken for each nanocomposite sample. The average values have been reported in the results.

3. Results and Discussion

3.1. IPN Formation

The IPN systems studied in this work comprise two resins with different curing mechanisms. It includes two independent curing reactions in the formation of IPNs, including epoxy resin (EP) and vinyl ester resin (VE), the step polymerization of EP with Methyltetrahydrophthalic Anhydride (MTHPA) as curing agent and 1-Methyl imidazole (Mi) as an accelerator, and the chain polymerization of VE initiated by MEKP as the initiator. Therefore, it is predictable to expect that we have encountered a multi-step curing mechanism. Our previous study 40 explored the interpenetration process of EP-MTHPA-Mi and VE-MEKP, as well as the interactions between

the components of epoxy and vinyl ester resin systems in IPN. Due to their different curing reactions, the EP-MTHPA-Mi/VE-MEKP systems are expected to exhibit sequential reactions, leading to sequential IPN formation. To study the thermal curing behavior of the epoxy (EP-MTHPA-Mi) and the vinyl ester (VE-MEKP), as well as their IPN (EP-MTHPA-Mi/VE-MEKP; 50/50 by weight), the curing process was investigated by DSC (see Figure 1). The DSC thermograms of the VE-MEKP system, the EP-MTHPA-Mi system, and the IPN system are shown in Figures 1a, 1b, and 1c, respectively. According to the DSC thermogram of the IPN system in Figure 1c, we observe a complex profile for its curing reaction, with a shoulder on the high-temperature side of the main exothermic peak. This shoulder indicates overlapping curing reactions between the two resin systems. The appearance of this shoulder, rather than entirely separate peaks, suggests that the epoxy and vinyl ester curing reactions occur in a sequential but overlapping manner during IPN formation.

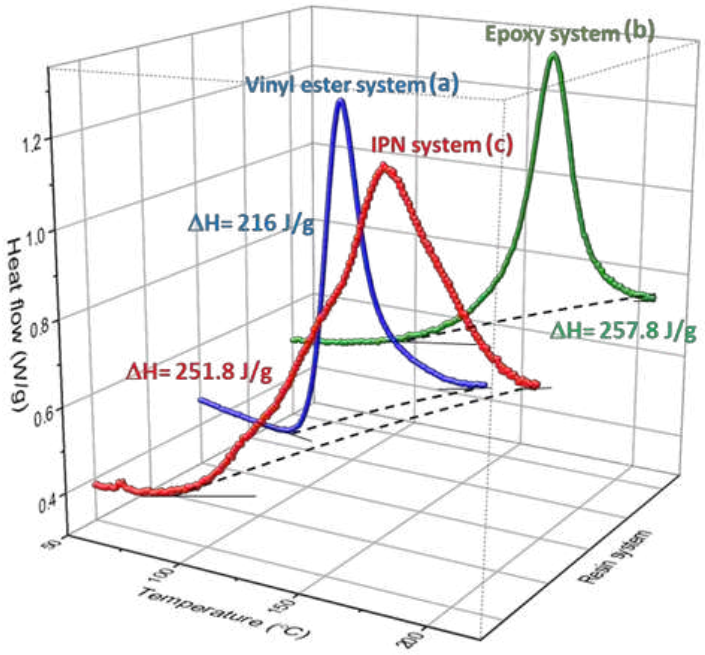


Figure 1. DSC thermograms of the VE-MEKP (a), the EP-MTHPA-Mi (b), and the IPN (c) systems.

The total heat of polymerization provides additional evidence of resin interaction during curing. According to the thermograms of the curing reactions, the IPN system shows the actual heat released (251.8 J/g), which is higher than the amount calculated from the weight-average of the individual components (257.8 × 0.50 + 216 × 0.50 = 236.9 J/g). This increase in heat release of approximately 15 J/g indicates additional chemical interactions between the epoxy and vinyl ester networks during simultaneous curing. These interactions include some reactions between the two polymer systems, contributing to the formation of a true interpenetrating network structure [40].

SEM images of the fracture surfaces of the EP-MTHPA-Mi/VE-MEKP IPN (50/50, by weight) samples after curing at 500 kx magnification have been evaluated to investigate the formation of an interpenetrating polymer network comprising epoxy and vinyl ester resins.

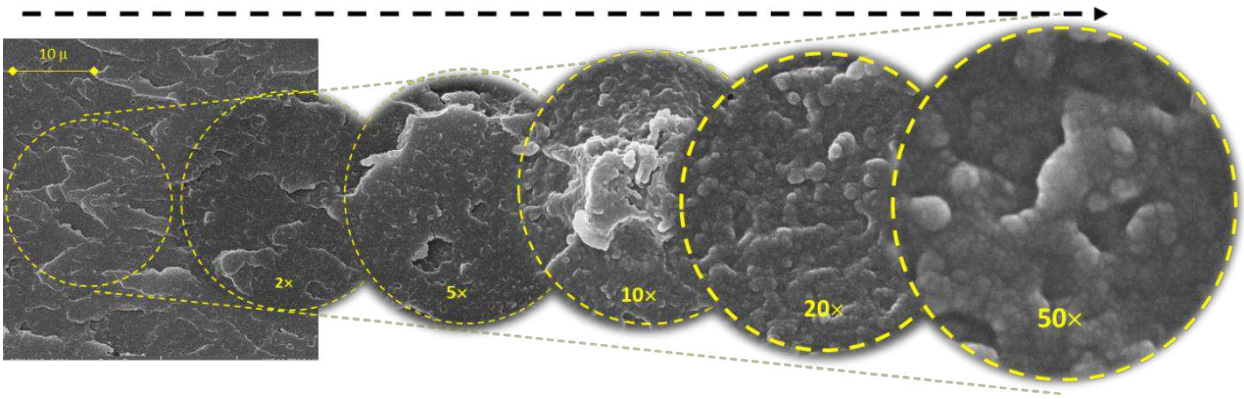


Figure 2. The fracture surface SEM micrograph of the EP-MTHPA-Mi/VE-MEKP IPN sample, highlighting structural features at increasing scales up to 50×.

As shown in Figure 2, the microstructure has a biphasic, co-continuous pattern with interconnected domains and granular, ribbon-like shapes. This complex structure, visible at both the micro- and nanoscales, is very different from the smooth, uniform structure of pure epoxy resins [15] and from the separate, nodular microgel structure observed in unmodified vinyl ester [15, 41]. The presence of these non-spherical, connected domains is a known sign of IPN formation in polymer blends [42].

3.2. Thermogravimetric Analysis (TGA) results

Thermogravimetric analysis was performed on unfilled and filled samples of EP-MTHPA-Mi, VE-MEKP, and their IPN systems. The filled samples, analyzed as nanocomposites, contained different weight percentages (0.01, 0.1, and 0.5) of GnPs and MWCNTs, either individually or in a 1:1 mixture. This analysis assessed component compatibility, confirmed the formation of IPN structures, and determined the thermal stability of the systems.

Figure 3 illustrates the TGA and DTG curves for all analyzed samples, with corresponding thermal degradation data presented in Table 2. All IPN-based samples exhibit similar degradation behavior patterns within the studied temperature range.

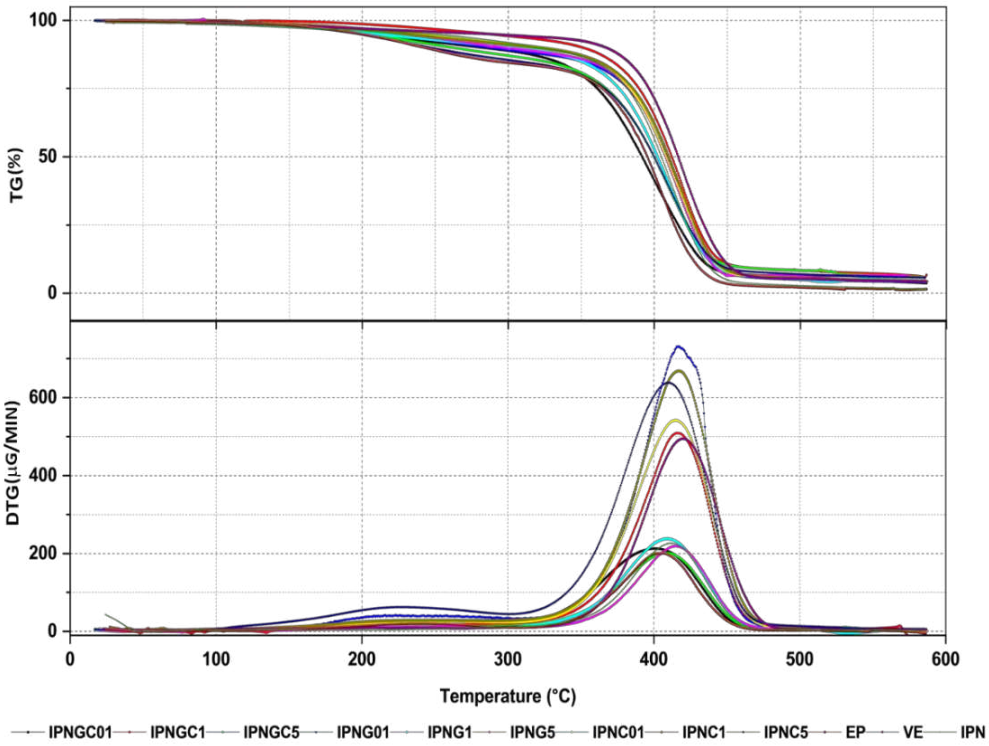


Figure 3. TGA (top) and DTG (bottom) curves for the samples.

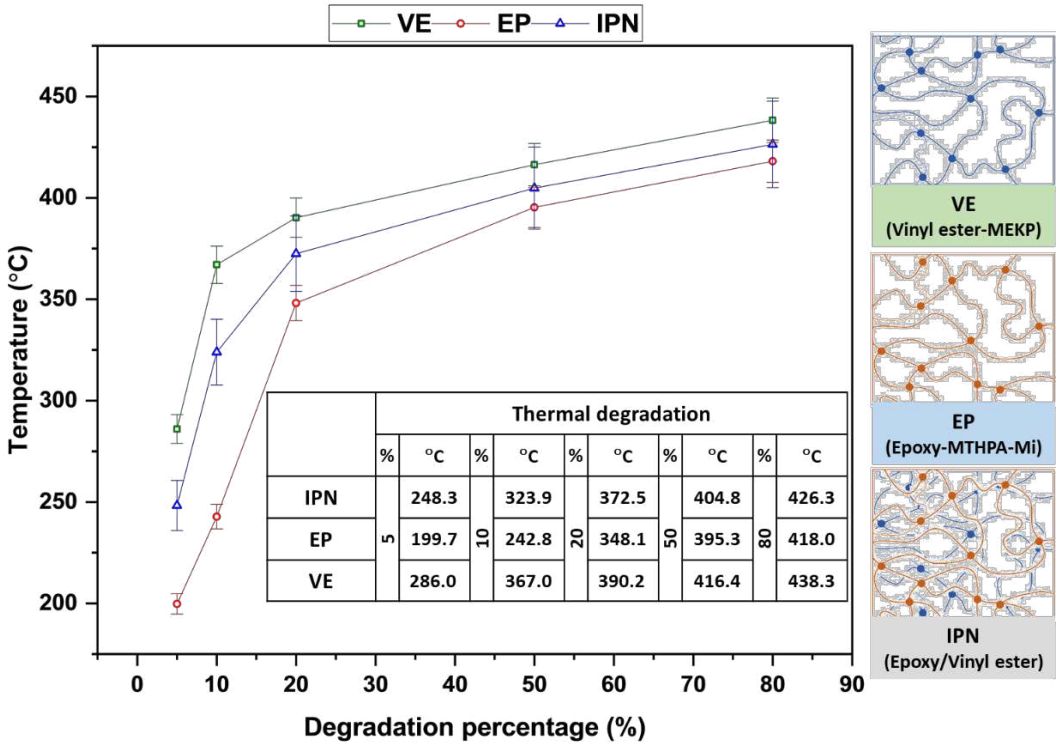
Table 2. Thermal degradation data of the samples.

No.	Sample	by DTG thermograms				Sample weight (mg)	by TGA thermograms				
		SAUC	T_{onset}	T_{peak}	T_{endset}		The temperature at the degradation of (°C)				
			(°C)				5%	10%	20%	50%	80%
1	IPNGC01	0.758	481.76	401.14	284.71	2.067	205.23	282.97	349.74	391.49	421.58
2	IPNGC1	0.780	478.71	416.87	320.03	3.688	286.46	351.04	382.01	411.74	433.16
3	IPNGC5	0.683	469.87	409.06	310.59	1.852	204.45	261.15	352.8	399.52	427.84
4	IPNG01	0.772	474.12	416.78	317.75	5.137	222.01	288.24	370.92	408.29	430.81
5	IPNG1	0.779	478.99	409.44	298.459	1.960	210.71	306.5	365.96	401.84	426.76
6	IPNG5	0.747	482.99	414.87	325.20	1.616	227.37	269.61	372.81	407.43	429.12
7	IPNC01	0.793	487.06	414.78	300.93	4.189	237.22	323.19	374.65	407.97	430.83
8	IPNC1	0.784	486.78	417.58	308.37	5.000	229.77	319.27	376.26	409.69	431.97
9	IPNC5	0.708	485.87	410.24	304.10	5.951	197.81	246.62	349.32	400.03	428.48
10	VE	0.857	487.74	414.22	315.26	3.512	274.95	355.98	379.21	405.35	427.25
11	EP	0.763	477.55	406.04	310.99	1.589	199.73	242.75	348.12	395.25	418.01
12	IPN	0.792	485.46	412.22	314.70	1.657	248.26	323.89	372.45	404.8	426.34

3.2.1. Comparative Analysis of Base Systems

By comparing the TGA thermograms of epoxy resin, vinyl ester, and IPN systems, we can see distinct patterns in their thermal degradation processes (see Figure 4). Weight loss temperature differences between VE and EP samples are most pronounced at lower degradation percentages: 75.22°C and 113.23°C at 5% and 10% weight loss, respectively. These differences decrease significantly at higher degradation levels, converging to approximately 9-10°C at 50% and 80%

weight loss. The IPN system consistently exhibits intermediate thermal behavior, with weight-loss temperatures falling between those of the individual EP and VE systems at all degradation percentages. At 80% weight loss, the IPN reaches 426.34°C, which is between the EP (418.01°C) and VE (427.25°C) values.



	Thermal degradation									
	%	°C	%	°C	%	°C	%	°C	%	°C
IPN	5	248.3	10	323.9	20	372.5	50	404.8	80	426.3
EP		199.7		242.8		348.1		395.3		418.0
VE		286.0		367.0		390.2		416.4		438.3

Figure 4. Weight-loss temperatures for IPN, EP, and VE Samples.

3.2.2. Early-Stage Weight Loss Characteristics

By evaluating the TGA thermogram of the cured EP-MTHPA-Mi resin system, a weight loss in the temperature range of 150 to 300 °C can be observed, which can be attributed to the removal of 1-methylimidazole (boiling point: 198 °C) used as a catalyst. This weight loss was absent in the cured VE-MEKP resin system at this temperature range and was less pronounced in the cured IPN system than in the cured epoxy system. These observations justify the temperature differences in the weight loss of 5% and 10% for these three cured resin systems.

3.3. DTG Analysis

DTG thermograms for pure IPN systems, epoxy resin (EP-MTHPA-Mi), and vinyl ester resin (VE-MEKP), along with the corresponding thermal stability metrics extracted from the DTG thermograms, namely, the Specific area under the DTG curve (SAUC) and the TG index (TGI), are presented in Fig. 5a and b. The DTG thermograms for all three resin systems exhibit single-peak behavior. The observation of identical thermal degradation behavior in the IPN compared to its resin components separately indicates the successful formation of the IPN without any detectable phase separation.

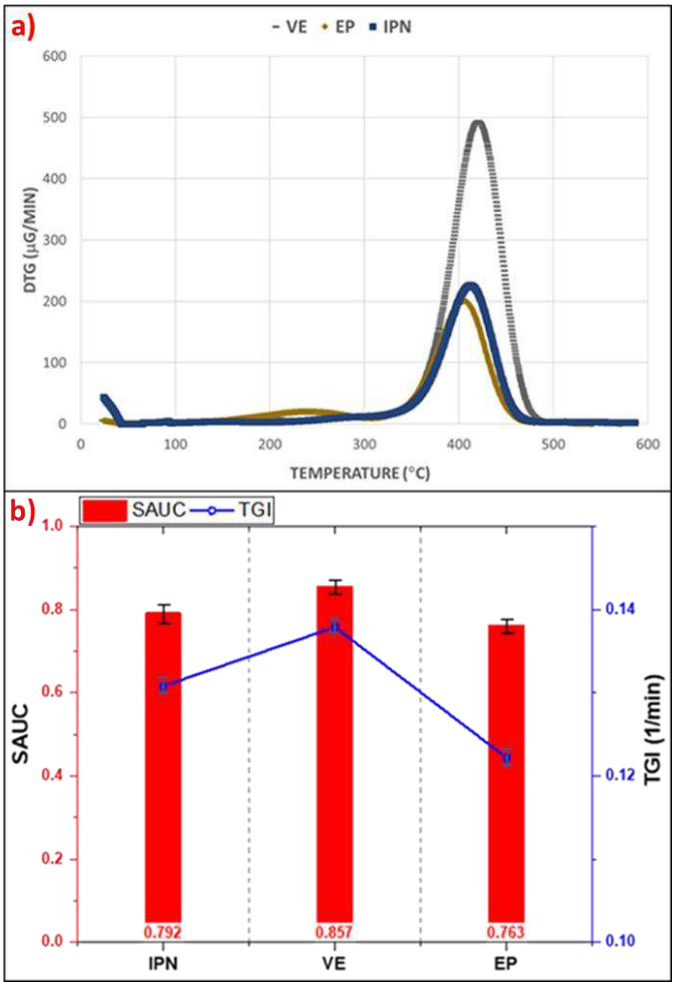


Figure 5. DTG curves (a), the specific area under the DTG curve, and the TG index (b) for IPN, EP, and VE Samples.

3.3.1. Thermal Degradation Characteristics

Three resin systems, including epoxy and vinyl ester, and their IPN exhibit different degradation temperature ranges and therefore distinct thermal behaviors:

- EP system: 310.99-477.55°C (ΔT_d = 166.56°C, peak at 406.04°C)
- VE system: 315.26-487.74°C (ΔT_d = 172.48°C, peak at 411.04°C)
- IPN system: 314.70-485.46°C (ΔT_d = 170.76°C, peak at 412.22°C)

The IPN exhibits intermediate thermal behavior between its constituent polymers, with degradation characteristics that are closer to those of the VE system.

3.3.2. Thermal Stability Assessment

Two parameters were used to quantify thermal stability and degradation kinetics:

Specific area under the DTG curve (SAUC) is calculated using the following equation [43, 44]:

$$SAUC = \frac{\Delta S}{\omega}$$

ΔS represents the area under the DTG curve, and ω is the initial sample weight. A larger area indicates better thermal stability within the degradation temperature range. The SAUC values indicate thermal stability ranking: VE (0.857) > IPN (0.792) > EP (0.763). The IPN shows 3.66% lower thermal stability than EP but 10.97% higher than VE.

TG index (TGI), another parameter derived from the DTG thermogram, measures the degradation rate of the samples and is calculated using the following equation [43, 44]:

$$TGI = \frac{\left[\frac{dW}{dt}\right]_{max}}{\omega}$$

$\left[\frac{dW}{dt}\right]_{max}$ is the maximum degradation rate based on the DTG curve. The TGI values follow the order: VE (0.1379) > IPN (0.1308) > EP (0.1222) min^{-1}, indicating that the IPN exhibits an

intermediate degradation rate between its components. The appearance of single-peak DTG thermograms across all nanocomposite systems confirms that nanofillers did not disrupt the formation of a homogeneous IPN structure. SAUC and TGI thermal stability measurements confirm that, upon forming an IPN, the thermal properties of the separate resin systems are well combined, resulting in a balanced performance between the constituent resin structures.

3.4. Effect of Nanoparticle Content and Type on Thermal Properties

The thermal behavior of IPN-based nanocomposites containing graphene nanoplatelets (GnPs), multi-walled carbon nanotubes (MWCNTs), and their 1:1 hybrid mixture (GnP/MWCNT) at 0.01, 0.1, and 0.5 wt% loadings was evaluated. Table 3 provides the complete sample coding system and nanoparticle content for all IPN-based nanocomposites.

Table 3. Coding and nanoparticle content of IPN-based nanocomposites.

No.	Code	Nanoparticles % wt.	Type and ratio of nanoparticles	
			MWCNTs	GnPs
1	IPN	0	0	0
2	IPNGC01	0.01	0.005	0.005
3	IPNGC1	0.1	0.05	0.05
4	IPNGC5	0.5	0.25	0.25
5	IPNG01	0.01	0	0.01
6	IPNG1	0.1	0	0.1
7	IPNG5	0.5	0	0.5
8	IPNC01	0.01	0.01	0
9	IPNC1	0.1	0.1	0

10	IPNC5	0.5	0.5	0

All nanocomposite systems exhibit single-peak DTG thermograms, confirming the maintenance of a homogeneous IPN structure regardless of the nanofiller type or concentration.

3.4.1. Content-Dependent Thermal Performance

Hybrid GnP/MWCNT Systems (IPNGC Series):

The temperatures corresponding to weight loss at different degradation levels for samples IPN, IPNGC01, IPNGC1, and IPNGC5 are shown in Figure 6. Optimal performance occurs at 0.1 wt% loading (IPNGC1), which shows superior weight-loss temperatures across all degradation percentages compared to both lower (IPNGC01) and higher (IPNGC5) concentrations. The IPNGC1 system exhibits enhanced thermal stability, with a degradation range of 158.68°C and a maximum degradation rate at 416.87°C. At 0.01 and 0.5 wt% loadings, thermal performance decreases below that of the pure IPN, suggesting concentration-dependent optimization effects: insufficient nanofiller loading fails to form effective thermal barriers. In contrast, excessive loading may lead to agglomeration.

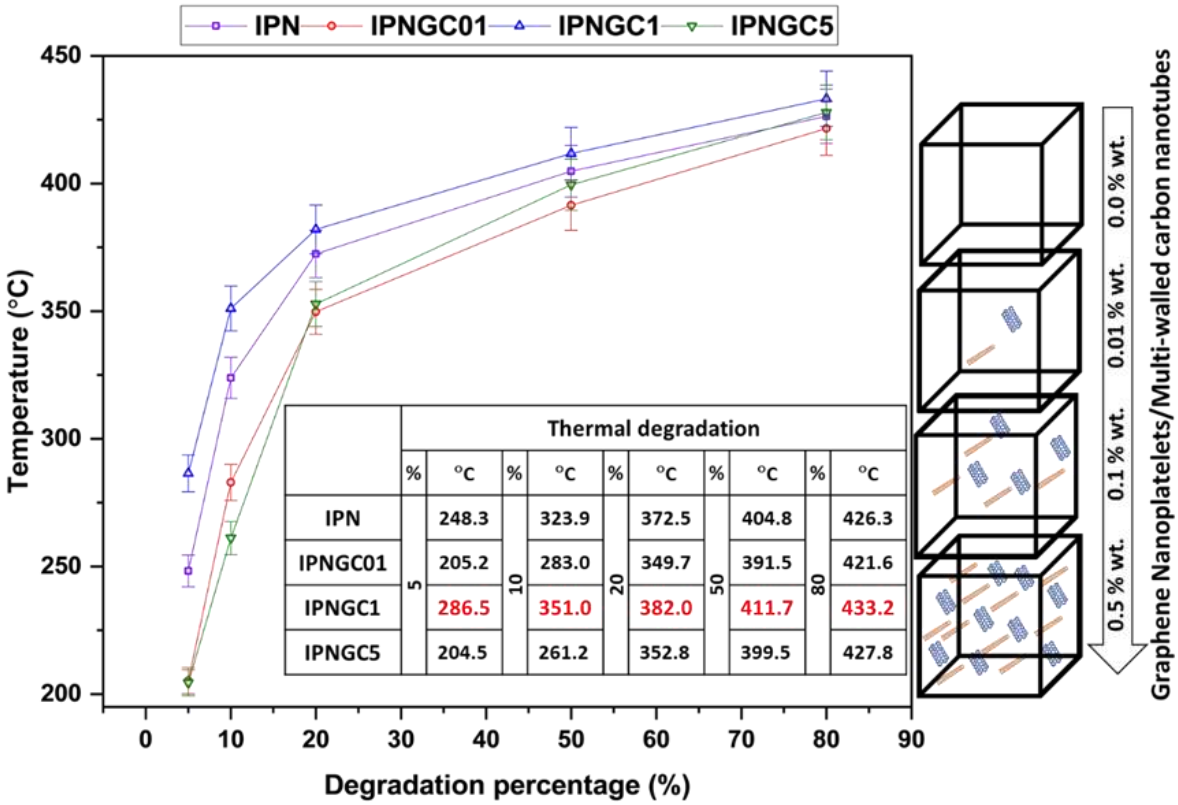
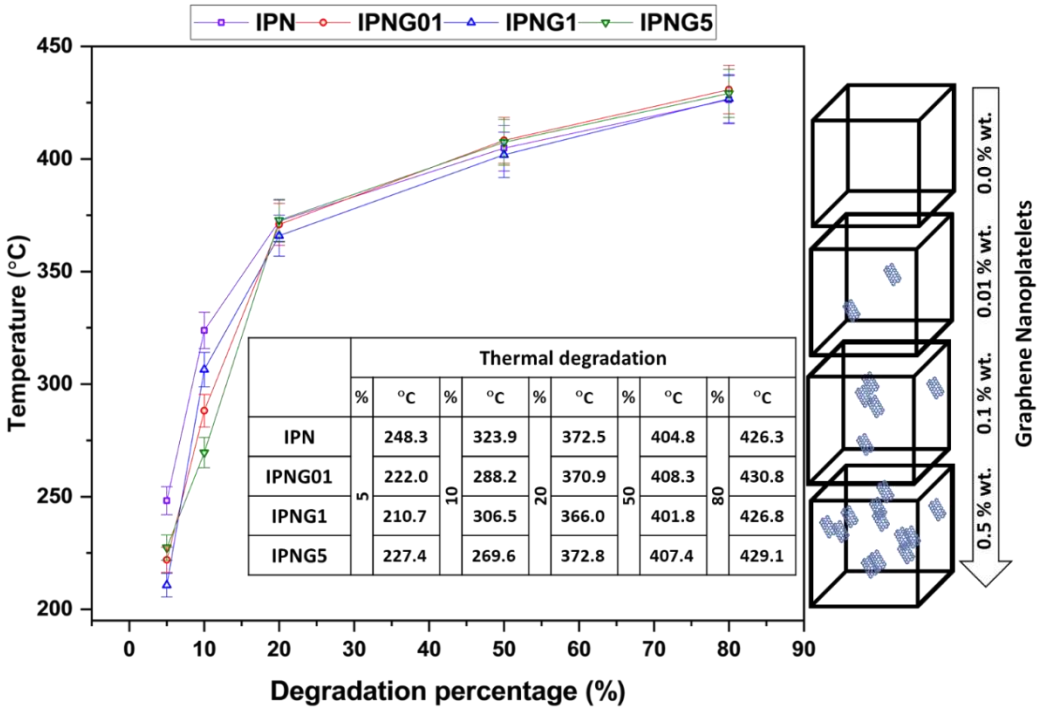


Figure 6. Weight-loss temperatures at different percentages of GnPs/MWCNTs for IPN, IPNGC01, IPNGC1, and IPNGC5 Samples.

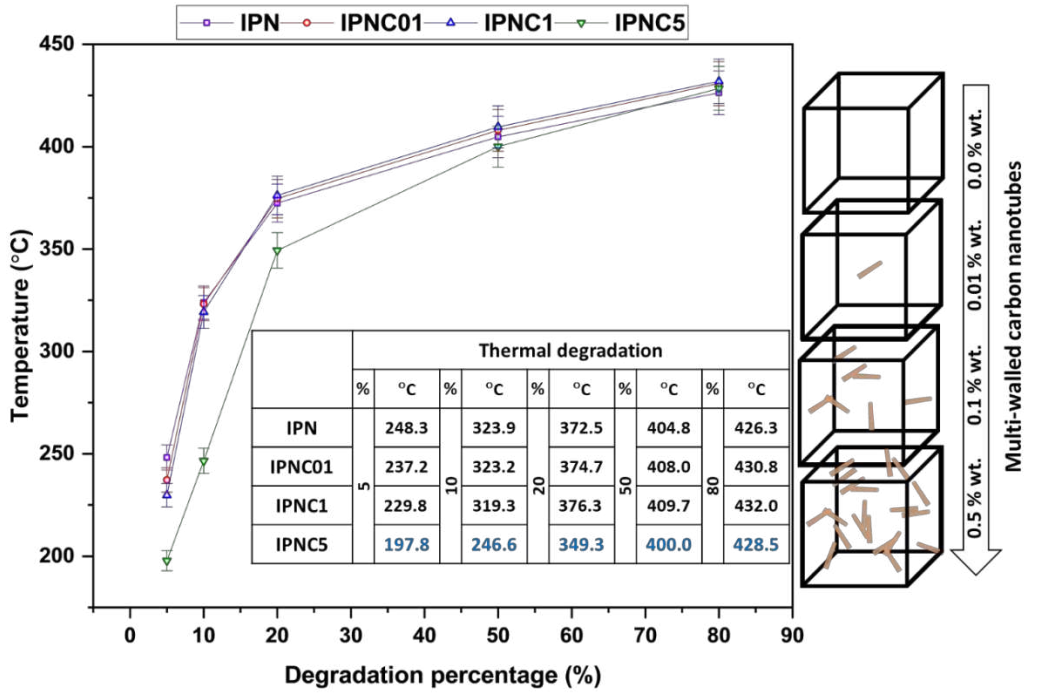
Individual Nanofiller Systems:

- GnP systems (IPNG series) required ≥0.5 wt% to match IPN thermal stability, with IPNG01 and IPNG5 outperforming IPNG1 by more than 20% in terms of degradation. Figure 7 shows the weight-loss temperatures at various degradation levels for IPN, IPNG01, IPNG1, and IPNG5.
- MWCNT systems (IPNC series) maintained consistent thermal performance across 0.01–0.5 wt%, with negligible differences in onset temperature at high degradation levels. Figure 8 shows the weight-loss temperatures at various degradation levels for IPN, IPNC01, IPNC1, and IPNC5.



	Thermal degradation									
	%	°C	%	°C	%	°C	%	°C	%	°C
IPN	5	248.3	10	323.9	20	372.5	50	404.8	80	426.3
IPNG01		222.0		288.2		370.9		408.3		430.8
IPNG1		210.7		306.5		366.0		401.8		426.8
IPNG5		227.4		269.6		372.8		407.4		429.1

Figure 7. Weight-loss temperatures at different percentages of GnPs for IPN, IPNG01, IPNG1, and IPNG5 Samples.



	Thermal degradation									
	%	°C	%	°C	%	°C	%	°C	%	°C
IPN	5	248.3	10	323.9	20	372.5	50	404.8	80	426.3
IPNC01		237.2		323.2		374.7		408.0		430.8
IPNC1		229.8		319.3		376.3		409.7		432.0
IPNC5		197.8		246.6		349.3		400.0		428.5

Figure 8. Weight-loss temperatures at different percentages of MWCNTs for IPN, IPNC01, IPNC1, and IPNC5 Samples.

3.4.2. Nanoparticle Type-Dependent Thermal Behavior

<u>Low nanofiller content (0.01 wt%):</u>

The IPN system containing a hybrid mixture of two nanofillers (IPNGC01) showed the widest degradation range (197.05°C) while exhibiting the lowest onset temperature for degradation. This is while IPN systems containing individual nanofillers at this level exhibited a higher degradation onset temperature and a narrower degradation temperature range.

Optimal nanofiller content (0.1 wt%):

At this nanofiller content, the IPN system containing a hybrid mixture of two nanofillers (IPNGC1) exhibited the highest weight-loss temperature across all degradation percentages, providing strong evidence of synergistic effects between GnPs and MWCNTs. The SAUC values for all three nanocomposites, IPNG1, IPNC1, and IPNGC1, are almost identical, indicating similar overall thermal stability.

Maximum nanofiller content (0.5 wt%):

At this nanofiller level, the IPN system containing only GnPs (IPNG5) presented the highest thermal stability with the lowest SAUC and the highest degradation onset temperature. These observations indicate that, at this nanofiller level, the planar geometry of GnPs provides better performance than combining GnPs and MWCNTs.

3.4.3. Thermal Stability Metrics Analysis

SAUC (Specific Area Under the DTG Curve): The lower the value of this parameter, the higher the thermal stability of the sample. The ranking varies based on the content of nanofillers:

- 0.01 wt%: IPNGC01 > IPNC01 > IPNG01
- 0.1 wt%: IPNGC1 ≈ IPNC1 ≈ IPNG1
- 0.5 wt%: IPNG5 > IPNGC5 > IPNC5

TGI (TG Index): This index measures the rate of thermal degradation; a lower value indicates a slower rate. The trend of this index mostly follows SAUC patterns and confirms the thermal stability ranking. Figure 9 presents the SAUC and TGI values for all samples across 3 parts.

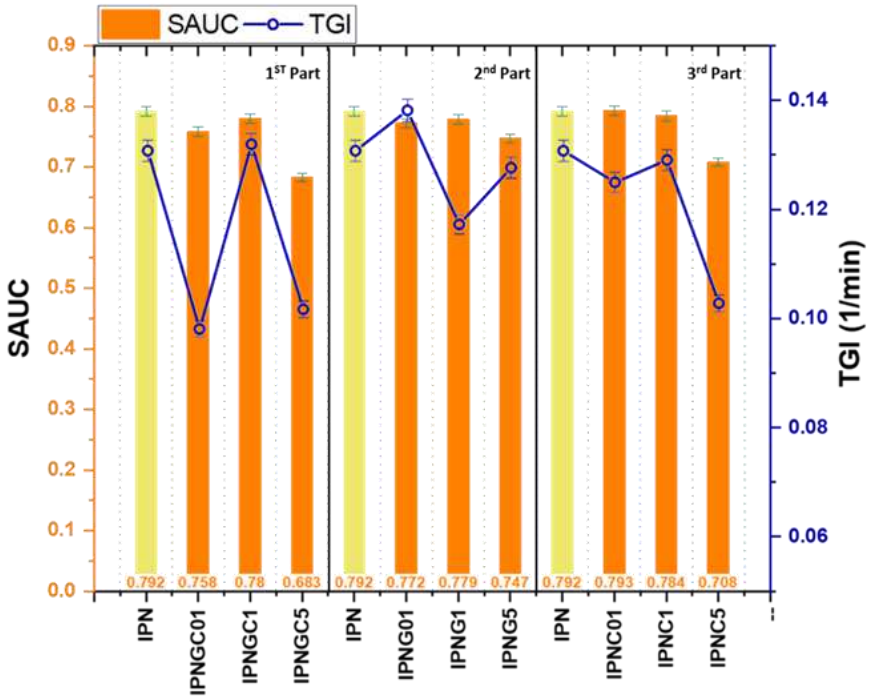
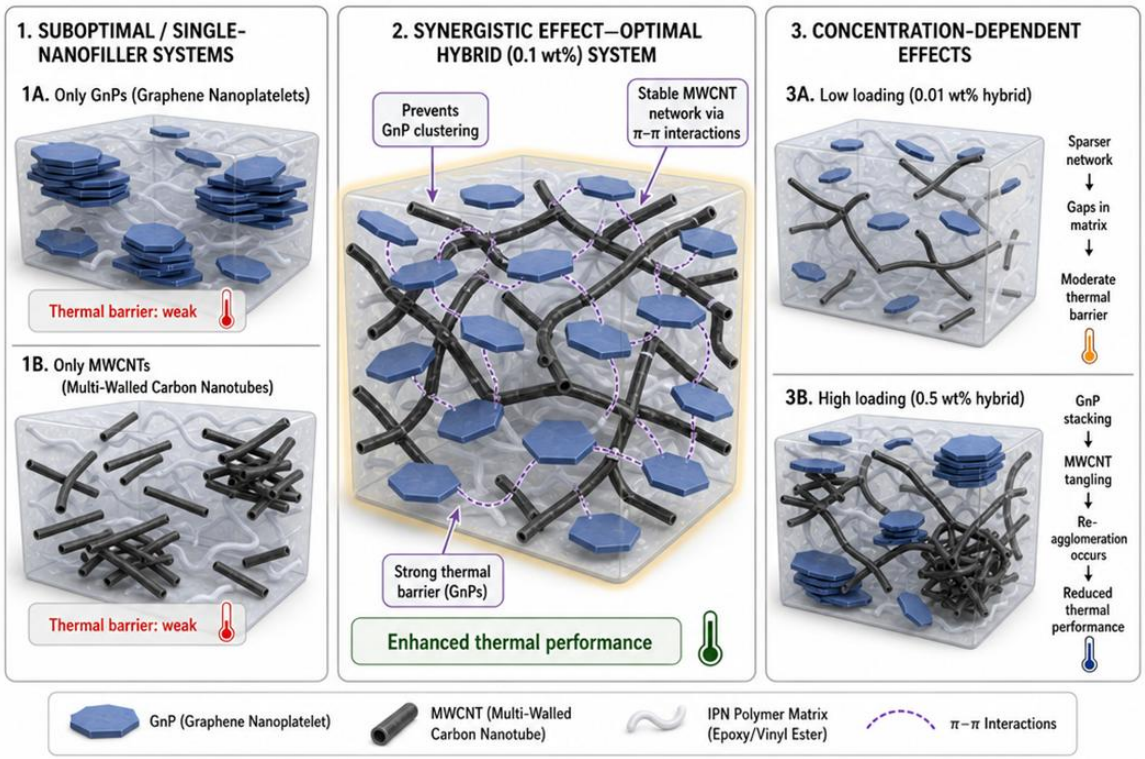


Figure 9. The specific areas under the DTG curves and the TG indices for (1st part) IPN, IPNGC01, IPNGC1, and IPNGC5; (2nd part) IPN, IPNG01, IPNG1, and IPNG5; and (3rd part) IPN, IPNC01, IPNC1, and IPNC5.

The evaluation of dispersion states in nanocomposite samples has been reported in our previous works 20, 31, and 40. The results of scanning electron microscopy (SEM) and dynamic mechanical thermal analysis (DMTA) in our research showed that incorporating only GnPs at 0.1 wt% or above led to some nanoparticle agglomeration, whereas incorporating only MWCNTs at 0.5 wt% or above led to clustering.

The simultaneous incorporation of MWCNTs and GnPs improved dispersion, resulting in a more uniform distribution and preventing nanoparticle agglomeration. In nanocomposites containing a mixture of these two nanofillers, MWCNTs formed an effective network, preventing the clustering of GnPs, resulting in uniform and stable dispersion and distribution. This led to improvements in

the nanocomposites' properties. In general, the most effective nanofiller network was obtained at an optimal loading of 0.1 wt% from the hybrid system of GnPs and MWCNTs, resulting in better thermal performance in the IPN-based nanocomposite samples.



Scheme 1. Dispersion behavior in GnPs and MWCNTs-filled IPN nanocomposites, showing agglomeration and clustering in single-filler systems and synergistic, uniform nanofiller distribution in the hybrid system at optimal 0.1 wt% loading.

An apparent synergistic effect is observed at this nanofiller weight percentage. In this system, the presence of plate-shaped GnPs leads to the formation of strong thermal barriers, while tubular MWCNTs form a stable network via π-π interactions (see Scheme 1). The result of these synergistic effects is an improvement in properties compared to samples containing only one nanofiller. Both samples containing 0.01 and 0.5 wt% of the nanofiller mixture show somewhat improved thermal stability. This fair improvement demonstrates that careful adjustment of nanofiller concentration is crucial to achieve sufficient improvement in thermal stability while preventing excessive aggregation. On the other hand, depending on the type of nanofiller, the

optimal concentration for improving the performance of the nanocomposite system varies: for GnPs nanofiller, the greatest effect is observed at higher loadings, whereas for MWCNTs nanofiller, performance remains relatively constant over the studied range. These observations emphasize the need to tailor the nanofiller type and content in epoxy/vinyl ester IPN nanocomposites to achieve optimal performance.

3.5. Effect of Nanoparticles on Fire Retardancy

Limiting oxygen index (LOI) values were estimated from TGA residue yields (CY) using the empirical relation, according to Van Krevelen's equation [45]:

$$LOI = 17.5 + 0.4CY$$

Table 4 lists the residue ash percentages (mean ± standard deviation, n = 3) and the corresponding LOI estimates. It should be noted that this calculation provides only an approximate measure of flame retardancy. The original correlation was developed for bulk polymers and does not account for differences in char morphology or the influence of nanofiller dispersion on gas-phase combustion processes. Moreover, the LOI values derived from TGA residues are subject to uncertainty from both the residual mass measurement (with a typical instrument precision of ±0.2 wt%) and the empirical nature of the formula, which may introduce an additional ±0.5% error.

Table 4. Residue ash content and LOI of the samples.

Sample	Residue ash (%)	LOI (%)
IPN	1.382	18.05
EP	1.477	18.09
VE	1.609	18.14
IPNC01	4.326	19.23

IPNC1	4.747	19.29
IPNC5	5.735	19.79
IPNG01	2.698	18.58
IPNG1	4.371	19.25
IPNG5	6.415	20.07
IPNGC01	3.674	18.97
IPNGC1	6.676	20.17
IPNGC5	5.841	19.84

As shown in Table 4, sample IPNGC1 (0.1 wt% GnP/MWCNT hybrid) showed the highest ash weight percentage (6.68 ± 0.03) and an estimated LOI of 20.17 ± 0.54, due to its superior char-formation capacity. Samples IPNG5 and IPNGC5, which contain 0.5 wt% GnPs and 0.5 wt% GnPs/MWCNTs mixture, respectively, are followed closely. The ash weight percentage and estimated LOI in sample IPNG5 are 6.42 ± 0.04 and 20.07 ± 0.53%, respectively, and in sample IPNGC5, they are 5.84 ± 0.02 and 19.84 ± 0.51%, respectively. Meanwhile, the epoxy, vinyl ester and unfilled IPN samples show higher ash weight percentage (1.38-1.61 ± 0.02) and estimated LOI values (18.05 ± 0.47-18.14 ± 0.47%). The optimal performance at 0.1 wt% loading of GnPs/MWCNTs mixture could be due to the char-barrier synergistic mechanisms, where the optimal arrangement of GnP nanoplaletts in the nanocomposite creates a tortuous diffusion path, while the MWCNT nanotubes contribute to the reinforcement of the char structure. At higher weight percentages, the formation of partial aggregation of GnPs could disrupt the structural

integrity of the formed char, leading to a slight increase in the estimated LOI. To validate these observations, direct LOI measurements and microscale combustion calorimetry are under investigation and will be reported in future work. These studies will quantify the influence of char structure and nanofiller dispersion on the actual flame behavior.

3.6. Microhardness test results

The microhardness test results for pure IPN (IPN), epoxy resin cured with MTHPA in the presence of 1-methylimidazole (EP), and vinyl ester resin cured with MEKP (VE) are presented. Additionally, the results for the nanocomposites based on this IPN, which contain three different weight percentages of 0.01, 0.1, and 0.5 GnPs and MWCNTs individually, as well as a one-to-one mixture of these two nanoparticles, were obtained using a standardized microhardness testing method, which can be found in Supporting Information Table 1s

Table 1s. Microhardness test results of the samples.

No.	Sample	Vickers microhardness HV (kgf/mm^2)	Image
1	IPNGC01	**23.4**	
2	IPNGC1	**22.4**	
3	IPNGC5	**22.1**	
4	IPNG01	**22.4**	
5	IPNG1	**22.9**	
6	IPNG5	**25.6**	
7	IPNC01	**23.2**	
8	IPNC1	**23.2**	

9	IPNC5	**23.2**	
10	VE	**9.8**	
11	EP	**24.8**	
12	IPN	**23.5**	

Figure 10 illustrates the microhardness values, which indicate the material's resistance to indentation or penetration, and the effective cross-link density (ν_c), for the pure IPN (IPN), the cured epoxy resin (EP), and the cured vinyl ester resin (VE). The effective cross-link density (ν_c) of the samples was determined as detailed in our earlier report [31].

According to the results, the lowest microhardness value is observed for the vinyl ester resin system (9.8 HV), and the highest is observed for the epoxy system (24.8 HV). These values suggest that the epoxy system is significantly harder than the vinyl ester system. When these two resin systems are combined in equal proportions and cured, the resulting IPN system exhibits a microhardness close to that of the epoxy system (23.5 HV), indicating that the IPN system has a hardness similar to that of the epoxy system.

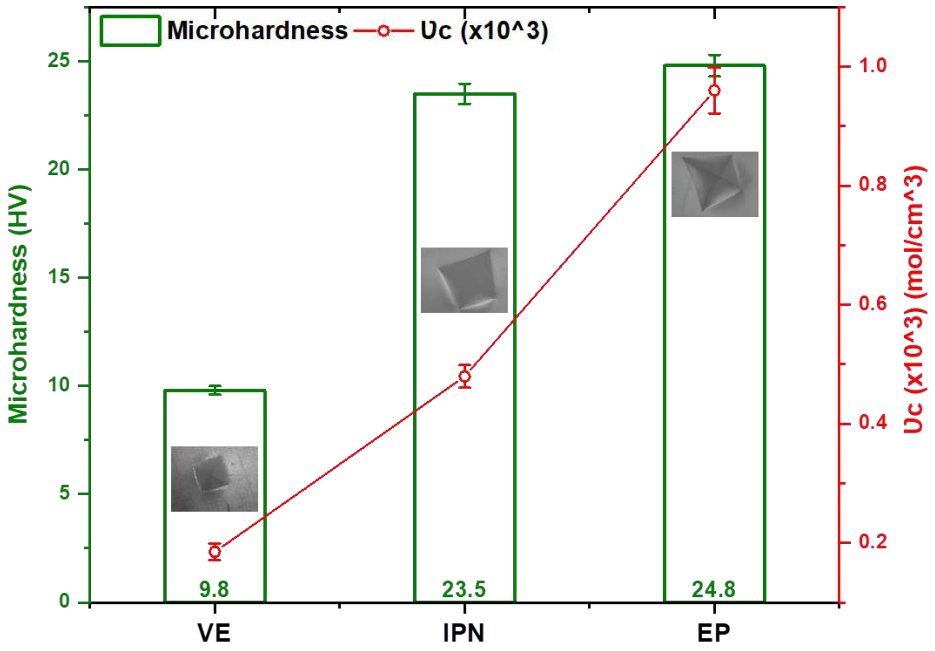


Figure 10. The microhardness and the effective cross-link density for IPN, EP, and VE.

Considering the increase of 0.7752 mmol/cm^3 in ν_c of EP compared to VE [31], the changes in the microhardness of the epoxy and vinyl ester systems seem reasonable. This trend in the IPN, due to the synergistic effects of these two resin networks, does not show a proportional relationship with its ν_c amount compared to the two resin systems. Despite the differences of 0.4806 and 0.2946 mmol/cm^3 between the ν_c of IPN and the values related to EP and VE [31], respectively, the microhardness of IPN is very close to that of the epoxy system.

3.7. The microhardness of the nanocomposites

Figure 11 illustrates a crucial aspect of our research: the microhardness levels of the nanocomposites. These levels are based on the EP/VE IPN system, which includes three different weight percentages of 0.01, 0.1, and 0.5 of GnPs and MWCNTs individually and a mixture of GnPs/MWCNTs.

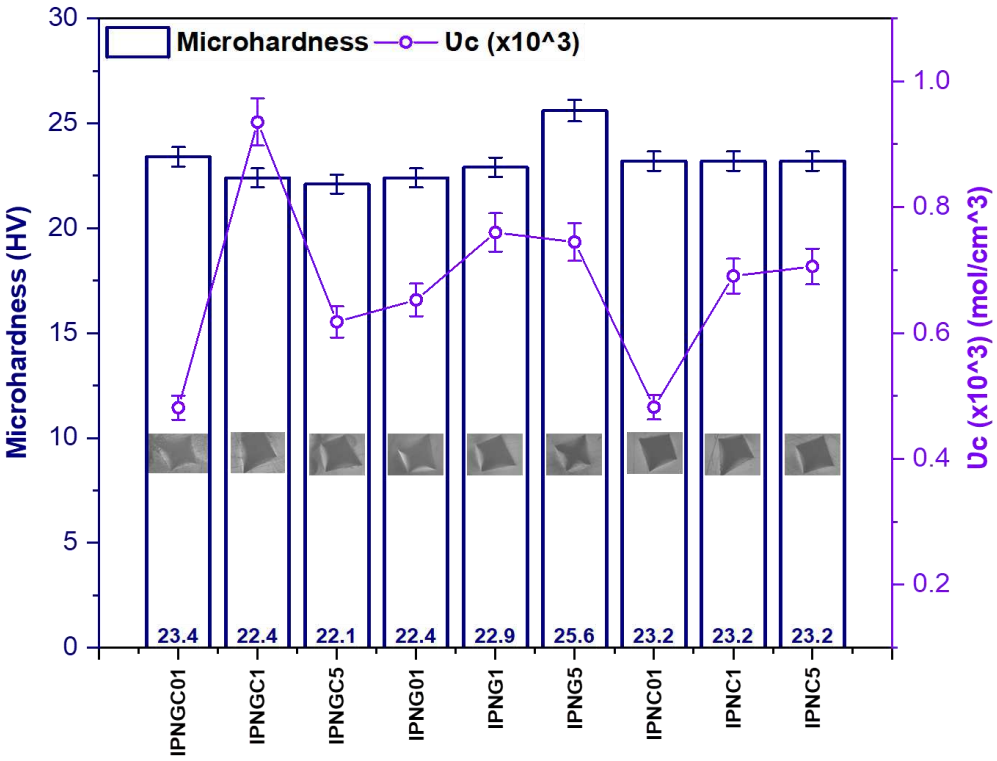


Figure 11. The microhardness and the effective cross-link density for the nanocomposite samples.

Based on Figure 11 and Table 1s, our comprehensive analysis reveals that the microhardness values of the cured nanocomposite samples, except for the IPNG5 sample, do not differ significantly. The IPNG5 sample, with the highest microhardness, suggests that a higher GnP content could be a contributing factor. The correlation between the microhardness of these nanocomposites and their effective cross-link density (ν_c) shows no direct dependence, suggesting that hardness is governed by both network architecture and nanofiller morphology rather than cure density alone [46].

Figure 12 presents the microhardness values alongside the temperature of the DTG peak extremum [Tp(DTG)] for the various samples analyzed. The vinyl ester sample exhibits the lowest microhardness, while the epoxy sample shows the lowest Tp(DTG). In contrast, the pure IPN sample composed of vinyl ester and epoxy depicts significant enhancements in microhardness and Tp values compared to the individual resin samples. These improvements highlight the synergistic

effects of combining vinyl ester and epoxy resins, as well as the formation of an IPN morphology, which contributes to the mechanical and thermal resistance of the samples. Furthermore, the incorporation of 0.01 and 0.1 wt% of a 1:1 combination of MWCNTs and GnPs into the IPN nanocomposites, designated as IPNCG01 and IPNCG1, respectively, leads to an increase in Tp(DTG) without adversely affecting the microhardness of these two samples compared to the pure IPN.

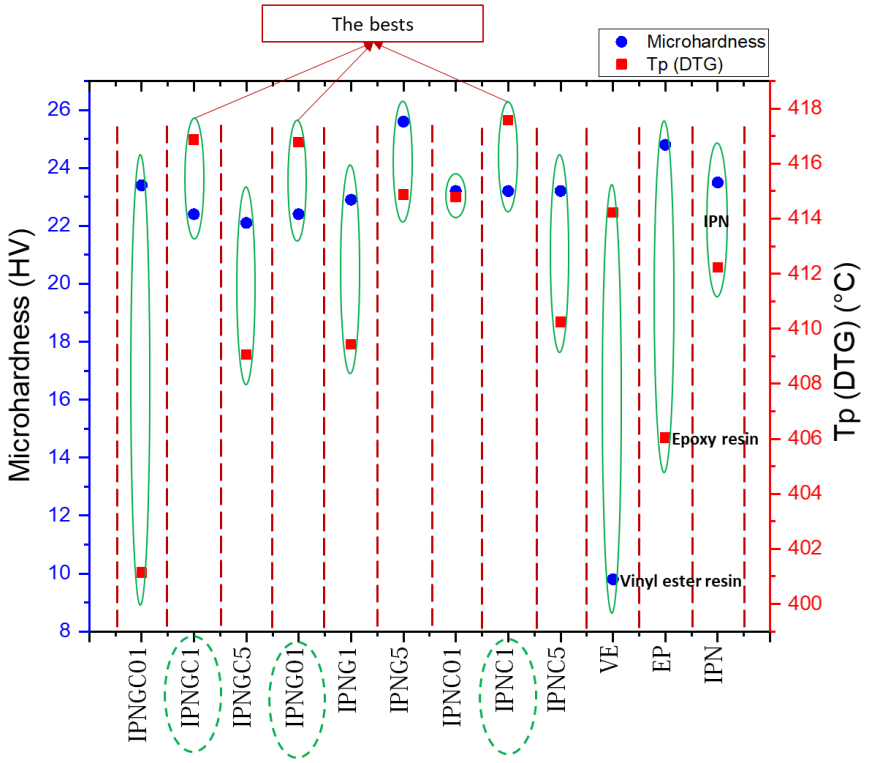


Figure 12. The microhardness values and the temperature of the DTG peak extremum [Tp (DTG)] for the samples.

Finally, the data presented in Figure 12 underscores the significant impact of resin composition and nanofiller on the mechanical and thermal properties of the nanocomposites. The significant enhancements in microhardness and thermal stability observed in the interpenetrating polymer network samples, particularly with the incorporation of multi-walled carbon nanotubes and graphene nanoplatelets, support the hypothesis that synergistic interactions among these materials

can lead to superior performance. These results indicate the potential to optimize nanocomposite materials by selecting material combinations to achieve optimal mechanical and thermal properties, creating a novel approach for advanced engineering and materials science applications.

4. Conclusion

This study demonstrates how the thermal properties of epoxy/vinyl ester IPN systems are enhanced through hybrid nanofillers. The research highlights the synergistic effects of combining GnPs and MWCNTs within the IPN matrix. It has been observed that IPN-based samples displayed similar degradation patterns. DTG thermograms of the EP/VE-based IPN showed a single peak, indicating a homogeneous system. This homogeneity is attributed to the compatibility between the epoxy and vinyl ester resins, facilitating the formation of a single-phase IPN. IPNGC1 (0.1 wt% GnP/MWCNT) exhibited the highest fire retardancy, with a limiting oxygen index (LOI) of 20.17 %. The microhardness of the IPN system was measured at 23.5 HV, which is close to that of the epoxy system (24.8 HV). Thermal stability was evaluated using the specific area under the DTG curve (SAUC), and the TG index (TGI) quantifies the sample's degradation rate within the temperature range of degradation. The study also explores how varying the type and content of nanoparticles impacts the thermal behavior of the resulting nanocomposites. TGA and DTG analyses evaluated thermal stability, degradation rates, and fire retardancy. The results indicate that incorporating hybrid nanofillers significantly influences the thermal stability and degradation patterns of the IPN. These findings emphasize the potential for optimizing nanocomposite materials by carefully selecting material combinations to enhance mechanical and thermal properties. The synergistic interactions observed in the IPN samples, particularly with multi-walled carbon nanotubes and graphene nanoplatelets, suggest the potential to achieve superior performance characteristics for advanced engineering and materials science applications.

Statements and Declarations

Authorship contributions statement

Afrooz Molaei: Data curation, Writing-original draft, Formal analysis, Methodology, Software.

Ali Jannesari: Project administration, Supervision, Writing-review & editing.

Funding and/or Conflicts of interest/Competing interests

The authors received no financial or other support from any organization for their work, and they have no personal or professional conflicts of interest that could in fluence the content of this article.

References

1. Mutch AL, Thickett SC. Mixed-mode interpenetrating polymer networks from polymerizable eutectics. Polymer Chemistry. 2025;16(12):1332-44. https://doi.org/10.1039/D4PY01456A

2. Shahi F, Zarei S, Salah Othman R, Afshar H, Kamran F, Afshar Taromi A, Khonakdar HA. Interpenetrating Polymer Networks in Biomedical Fields: Recent Advanced and Applications. Polymers for Advanced Technologies. 2025;36(2):e70099. https://doi.org/10.1002/pat.70099

3. Farooq U, Teuwen J, Dransfeld C. Toughening of epoxy systems with interpenetrating polymer network (IPN): A review. Polymers. 2020;12(9):1908. https://doi.org/10.3390/polym12091908

4. Vallittu PK. Interpenetrating polymer networks (IPNs) in dental polymers and composites. *Journal of Adhesion Science and Technology*. 2009;23(7-8):961-972. https://doi.org/10.1163/156856109X432785

5. Ding W, Zhao Z, Jiang L, Jian X, Song Y, Wang J. Preparation and evaluation of a UV-curing hydrophilic semi-IPN coating for medical guidewires. *Journal of Coatings Technology and Research*. 2021;18:1027-1035. https://doi.org/10.1007/s11998-020-00455-9

6. Liu S, Liu S, Wang Q, Zuo Z, Liang X. Design and synthesis of robust superhydrophobic coating based on epoxy resin and polydimethylsiloxane interpenetrated polymer network. *Progress in Organic Coatings*. 2023;175:107336. https://doi.org/10.1016/j.porgcoat.2022.107336

7. Cai M, Lin Q, Li W, Fan X, Zhu M. Phen@ TiO_2 modified epoxy resin/polyacrylate IPN composite coating towards wear/corrosion resistance and intelligent self-repairing/diagnosis. *Progress in Organic Coatings*. 2022;173:107207. https://doi.org/10.1016/j.porgcoat.2022.107207

8. Gao M, Zhao J, Wang G, Jin H, Wang J, Tian L. High adhesive and mechanically stable SR/PU IPNs coating with dual-functional antifouling/anticorrosive performances. *Progress in Organic Coatings*. 2023;176:107385. https://doi.org/10.1016/j.porgcoat.2022.107385

9. Wancura M, Nkansah A, Chwatko M, Robinson A, Fairley A, Cosgriff-Hernandez E. Interpenetrating network design of bioactive hydrogel coatings with enhanced damage resistance. *J Mater Chem B*. Feb 24, 2023. https://doi.org/10.1039/D2TB02825E

10. Cona C, Bailey K, Barker E. Characterization methods to determine interpenetrating polymer network (IPN) in hydrogels. Polymers. 2024;16(14):2050. https://doi.org/10.3390/polym16142050

11. Valderruten NE, García J. Interpenetrating polymer networks of poly (2-hydroxyethyl methacrylate co-itaconic acid) and chitosan as a controlled release matrix. Reactive and Functional Polymers. 2025:106192. https://doi.org/10.1016/j.reactfunctpolym.2025.106192

12. Sperling LH. Interpenetrating polymer networks and related materials. Springer Science & Business Media; 2012. https://doi.org/10.1007/978-1-4684-3830-7

13. Utracki LA, Wilkie CA, editors. Polymer blends handbook. Dordrecht: Kluwer academic publishers; 2002 Dec.

14. Dean KM, Cook WD, Lin MY. Small angle neutron scattering and dynamic mechanical thermal analysis of dimethacrylate/epoxy IPNs. European polymer journal. 2006;42(10):2872-87. https://doi.org/10.1016/j.eurpolymj.2006.04.013

15. Karger-Kocsis J, Gryshchuk O, Schmitt S. Vinylester/epoxy-based thermosets of interpenetrating network structure: An atomic force microscopic study. Journal of materials science. 2003;38:413-20. https://doi.org/10.1023/A:1021855228253

16. Dean K, Cook WD, Rey L, Galy J, Sautereau H. Near-infrared and rheological investigations of epoxy−vinyl ester interpenetrating polymer networks. Macromolecules. 2001;34(19):6623-30. https://doi.org/10.1021/ma010438z

17. Szabó JS, Gryshchuk O, Karger-Kocsis J. Fatigue crack propagation behavior of interpenetrating vinylester/epoxy resins. Journal of Materials Science Letters. 2003;22(16). https://doi.org/10.1023/A:1025175027424

18. Gryshchuk O, Karger-Kocsis J. Influence of the type of epoxy hardener on the structure and properties of interpenetrated vinyl ester/epoxy resins. Journal of Polymer Science Part A: Polymer Chemistry. 2004 ;42(21):5471-81. https://doi.org/10.1002/pola.20371

19. Turcsan T, Meszaros L. Mechanical performance of hybrid thermoset composites: Effects of matrix and reinforcement hybridization. Composites Science and Technology. 2017;141:32-9. https://doi.org/10.1016/j.compscitech.2017.01.005

20. Molaei A, Jannesari A. The synergistic impacts of hybrid nanofillers of graphene nanoplatelets/carbon nanotubes on curing behavior of an epoxy-vinyl ester interpenetrating polymer network nanocomposite coating. Polymer Composites. 2023;44(11):7701-26. https://doi.org/10.1002/pc.27657

21. Karger-Kocsis J, Gryshchuk O, Fröhlich J, Mülhaupt R. Interpenetrating vinylester/epoxy resins modified with organophilic layered silicates. Composites Science and Technology. 2003;63(14):2045-54. https://doi.org/10.1016/S0266-3538(03)00110-6

22. Szabo JS, Romhány G, Czigány T, Karger-Kocsis J. Interpenetrating vinyl ester/epoxy resins reinforced by flax fibre mat. Advanced Composites Letters. 2003;12(3):096369350301200304. https://doi.org/10.1177/096369350301200304

23. Szabo JS, Karger-Kocsis J, Gryshchuk O, Czigány T. Effect of fibre surface treatment on the mechanical response of ceramic fibre mat-reinforced interpenetrating vinylester/epoxy resins. Composites science and technology. 2004;64(10-11):1717-23. https://doi.org/10.1016/j.compscitech.2004.01.006

24. Czigány T, Pölöskei K, Karger-Kocsis J. Fracture and failure behavior of basalt fiber mat-reinforced vinylester/epoxy hybrid resins as a function of resin composition and fiber surface treatment. Journal of materials science. 2005;40:5609-18. https://doi.org/10.1007/s10853-005-1273-8

25. Mészáros L, Turcsán T. Development and mechanical properties of carbon fibre reinforced EP/VE hybrid composite systems. Periodica Polytechnica Mechanical Engineering. 2014;58(2):127-33. https://doi.org/10.3311/PPme.7237

26. Turcsan T, Meszaros L. Mechanical performance of hybrid thermoset composites: Effects of matrix and reinforcement hybridization. Composites Science and Technology. 2017;141:32-9. https://doi.org/10.1016/j.compscitech.2017.01.005

27. Hiremath MM, Ray BC, Prusty RK. Improved mechanical responses of GFRP composites with epoxy-vinyl ester interpenetrating polymer network. Polymer Testing. 2021;93:107008. https://doi.org/10.1016/j.polymertesting.2020.107008

28. Gryshchuk O, Karger-Kocsis J, Thomann R, Kónya Z, Kiricsi I. Multiwall carbon nanotube modified vinylester and vinylester–based hybrid resins. Composites Part A: Applied Science and Manufacturing. 2006;37(9):1252-9. https://doi.org/10.1016/j.compositesa.2005.09.003

29. Lungu A, Florea NM, Damian CM, Iovu H. Thermo-mechanical properties of interpenetrating polymer networks (IPNS) filled with fumed silica nanoparticles. Materiale Plastice. 2011;3:209-13.

30. Sen B, Hiremath MM, Prusty RK, Ray BC. Enhanced creep resistance of GFRP composites through interpenetrating polymer network. International Journal of Mechanical Sciences. 2021;212:106728. https://doi.org/10.1016/j.ijmecsci.2021.106728

31. Molaei A, Jannesari A. Study on structure and viscoelastic behavior of epoxy/vinyl ester interpenetrating polymer network nanocomposites containing graphene nanoplatelets/multi-wall carbon nanotubes. Polymer Engineering & Science. 2025;1-14. https://doi.org/10.1002/pen.27070

32. Yang J, Zhang Y, Hao M, Zhi J, Qian X. Synergistically toughened epoxy resin based on modified-POSS triggered interpenetrating network. Polymer. 2023;268:125719. https://doi.org/10.1016/j.polymer.2023.125719

33. Dean K, Cook WD, Rey L, Galy J, Sautereau H. Near-infrared and rheological investigations of epoxy−vinyl ester interpenetrating polymer networks. Macromolecules. 2001;34(19):6623-30. https://doi.org/10.1021/ma010438z

34. Afolabi OA, Ndou N. Synergy of hybrid fillers for emerging composite and nanocomposite materials—a review. Polymers. 2024;16(13):1907.https://doi.org/10.3390/ma12020255

35. Wang H, Xiao E, Fan T, Li X, Xiao W. Calculations of factors that affect thermal conductivity in epoxy composites with hybrid carbon nanotube and graphene nano platelet. Materials Research Express. 2020;7(2):025031. https://doi.org/10.1088/2053-1591/ab71ca

36. Jen YM, Huang JC. Synergistic effect on the thermomechanical and electrical properties of epoxy composites with the enhancement of carbon nanotubes and graphene nano platelets. Materials. 2019;12(2):255. https://doi.org/10.3390/ma12020255

37. Yang SY, Lin WN, Huang YL, Tien HW, Wang JY, Ma CC, Li SM, Wang YS. Synergetic effects of graphene platelets and carbon nanotubes on the mechanical and thermal properties of epoxy composites. Carbon. 2011;49(3):793-803. https://doi.org/10.1016/j.carbon.2010.10.014

38. Lago E, Toth PS, Pugliese G, Pellegrini V, Bonaccorso F. Solution blending preparation of polycarbonate/graphene composite: boosting the mechanical and electrical properties. RSC advances. 2016;6(100):97931-40. https://doi.org/10.1039/C6RA21962D

39. Cheng X, Kumar V, Yokozeki T, Goto T, Takahashi T, Koyanagi J, Wu L, Wang R. Highly conductive graphene oxide/polyaniline hybrid polymer nanocomposites with simultaneously improved mechanical properties. Composites Part A: Applied Science and Manufacturing. 2016 Mar 1;82:100-7. https://doi.org/10.1016/j.compositesa.2015.12.006

40. Molaei A, Jannesari A. The synergistic impacts of hybrid nanofillers of graphene nanoplatelets/carbon nanotubes on curing behavior of an epoxy-vinyl ester interpenetrating polymer network nanocomposite coating. Polymer Composites. 2023 Nov;44(11):7701-26. https://doi.org/10.1002/pc.27657

41. Ganglani M, Torkelson J, Carr S. Polymerization-Induced Phase Separation in Vinyl Ester Resins. In

American Physical Society, March Meeting Abstracts 2000 Mar (pp. L36-162).

42. Dean K, Cook WD, Burchill P, Zipper M. Curing behaviour of IPNs formed from model VERs and epoxy systems: Part II. Imidazole-cured epoxy. Polymer. 2001 Apr 1;42(8):3589-601. https://doi.org/10.1016/S0032-3861(00)00745-X

43. Camino G, Costa L. Performance and mechanisms of fire retardants in polymers—a review. Polymer Degradation and Stability 1988; 20:271–294. https://doi.org/10.1016/0141-3910(88)90073-0

44. Bakirtzis D.S., Tsapara V.C., K. G. Kolovos K.G. and Liodakis S.E., Assessment of the impact of fire retardants on the combustion of natural polymers employing DTG and LOI, Fire Mater. 2015; 39:109–118. https://doi.org/10.1002/fam.2232

45. Van Krevelen DW, Te Nijenhuis K. Properties of polymers: their correlation with chemical structure; their numerical estimation and prediction from additive group contributions. Elsevier; 2009 Feb 9; 847-873.

46. Bayraktar ET, Atali PY, Korkut B, Kesimli EG, Tarcin B, Turkmen C. Effect of modeling resins on microhardness of resin composites. European Journal of Dentistry. 2021;15(03):481-7. https://doi.org/10.1055/s-0041-1725577

Supplementary Files

This is a list of supplementary files associated with this preprint. Click to download.

- Supportinginformation.docx